A New Adaptive Neural Fuzzy Sliding Control Method for Dynamic Nonlinear Plants

Nguyen Anh Tuan [1,2,3] and Ho Pham Huy Anh [1,2,*]

[1] Ho Chi Minh City University of Technology (HCMUT), 268 Ly Thuong Kiet, Dien Hong Ward, Ho Chi Minh City, Viet Nam
[2] Vietnam National University Ho Chi Minh City (VNU-HCM), Tan Lap Quarter, Dong Hoa Ward, Ho Chi Minh City, Viet Nam
[3] Faculty of Engineering and Technology, Sai Gon University (SGU), 273 An Duong Vuong Street, Cho Quan Ward, Ho Chi Minh City, Viet Nam
Email: nguyenanhtuan.sdh21@hcmut.edu.vn, natuan@sgu.edu.vn (N.A.T.); hphanh@hcmut.edu.vn (H.P.H.A.)
*Corresponding author

***Abstract*—This paper proposes a New Adaptive Neural Fuzzy Sliding Mode Controller (NANFSMC) for regulating a Coupled Tank System (CTS), with unknown nonlinear dynamics in experimental environments. The CTS exhibits strong nonlinearities and uncertainties arising from sensor noise, parameter variations, variations in output valve characteristics, and significant time delays. The proposed control architecture integrates two synergistic components. The first component is an adaptive control system that utilizes a Radial Basis Function Neural Network (RBFNN) to approximate the adaptive control law, featuring an adaptive updating mechanism to compensate for RBFNN approximation errors. The second component is a Sliding Mode Control (SMC) system, whose parameters are updated in real-time via a fuzzy inference mechanism to enhance robustness. Both control laws are derived within the framework of Lyapunov stability theory, ensuring closed-loop stability under all operating conditions. The proposed controller possesses a simple structure, resulting in low computational load and requiring only a few tuning parameters. Although the RBFNN weights are initialized to 0, the integration with the adaptive fuzzy mechanism allows fast convergence and rapid stabilization. Furthermore, this study presents the first experimental validation of a Takagi-Sugeno (TS)-fuzzy–based adaptive tuning of the SMC robustness gain on a real CTS under external disturbances. The proposed method achieves improvements of up to 22.9% and 14.2% in the Integral of Absolute Error (IAE), Mean Absolute Error (MAE), and Integral of Time-weighted Absolute Error (ITAE) indices compared to the Adaptive Neural SMC (ANSMC) and Proportional Integral Derivative (PID) controllers, respectively.**

***Keywords*—Proportional Integral Derivative (PID), approximation error, real-time validation, external disturbance, robustness, computational load**

I. Introduction

Accurate liquid-level regulation in process tanks is essential in industrial production, as it directly impacts process efficiency and product quality. In particular, liquid-level control in chemical manufacturing, oil and gas processing, and food production requires high precision and reliability. These systems typically exhibit nonlinear dynamics and significant uncertainties, including sensor noise, variations in outlet valve cross-sections, environmental changes, actuator nonlinearities, and considerable time delays. The Coupled Tank System (CTS) is widely used in laboratory environments as a benchmark for studying liquid-level control. It replicates the nonlinear characteristics, uncertainties, and high time delays in industrial processes. Consequently, a broad spectrum of control strategies—ranging from classical to advanced—has been investigated to evaluate control performance on the CTS.

Initial studies [1, 2] applied Proportional Integral Derivative (PID) controllers to address the slow dynamic response of CTS. A robust Sliding Mode Control (SMC) scheme is introduced in Ref. [3] to mitigate nonlinearities and reduce the influence of disturbances and noise. Al-Majeez *et al.* [4] proposed a backstepping control approach for an interconnected twin-tank system. Simulation results demonstrated that the backstepping controller exhibited higher robustness than the synergetic controller against external disturbances. However, the results were only verified through simulations with step-type reference inputs; hence, the actual robustness performance has not yet been experimentally validated. Furthermore, this control algorithm depends on the dynamic model of the system, which may limit its applicability to systems with modeling uncertainties. Subsequently, Aranda-Cetraro *et al.* [5] combined backstepping, super-twisting, and the modulating function technique to eliminate the dependency on state derivatives. This approach also helps suppress measurement noise and mitigating the chattering phenomenon in a Quadruple-Tank System (QTS). Simulation results under non-Gaussian measurement noise and varying reference

Manuscript received September 8, 2025; revised October 29, 2025; accepted December 3, 2025; published February 9, 2026.

signals confirmed good tracking capability and reduced chattering. Nevertheless, these results are also limited to simulations, and thus, the practical effectiveness of the method remains unverified.

In addition, disturbance observer-based methods [6–8] and active disturbance rejection control [9] are also proposed to suppress external perturbations in liquid-level systems. Moreover, SMC is integrated with adaptive control techniques [10] for liquid-level regulation in QTS, yielding improved robustness to reference variations and external disturbances. However, except for PID-based methods, most of these approaches rely on accurate plant models, often unavailable or subject to significant variation during operation. This limitation reduces the practical applicability of model-based control methods.

As a result, it motivates the adoption of model-free and Artificial Intelligence (AI) integrated strategies. In this direction, Abushokor and Amrr [11] proposed a model-free adaptive time-delay estimation method for CTS control, requiring only historical input-output data to estimate system behavior and embed it into a robust control framework. A fuzzy Proportional-Integral (PI) controller with s- and z-type membership functions [12] is developed to enhance robustness against uncertainties, outperforming conventional fuzzy PI methods. Furthermore, Bhandare *et al.* [13] introduces an intelligent fuzzy fractional-order PI controller to improve performance.

Hybrid approaches that combine AI techniques with advanced control strategies have also gained attention. For instance, SMC combined with Recurrent Neural Networks (RNNs) [14] adaptively updates the equivalent control term and sliding surface online to reduce chattering. An adaptive fuzzy SMC scheme [15] is proposed to handle external noise and actuator faults. In contrast, an adaptive inverse multilayer Takagi-Sugeno (TS) fuzzy controller [16] employs differential evolution optimization for uncertain nonlinear Single-Input Single-Output (SISO) systems. However, it relies on offline parameter identification. Adaptive neural SMC methods are explored to enhance stability and performance in the presence of nonlinearities and unknown disturbances [17, 18]. In Ref. [17], an adaptive neural controller is integrated with SMC to estimate nonlinearities and uncertainties online. In contrast, Li *et al.* [18] develops an adaptive neural SMC for nonlinear SISO systems with unknown dynamics, focusing on chattering suppression. Refs. [19, 20] further improve tracking performance by using RNN-based adaptive neural SMC to estimate model uncertainties and external perturbations, enabling faster tracking error convergence. Ref. [21] combined an adaptive neural SMC algorithm with backstepping to approximate the nonlinear aerodynamic forces and moments of an aircraft.

Meanwhile, the adaptive backstepping terminal sliding mode control utilizes a physics-informed neural network [22] to accurately estimate and compensate for system uncertainty. Recent works [23–26] leverage the fast approximation capability of Radial Basis Function Neural Networks (RBFNN) and the strong robustness of SMC to develop an Adaptive Neural SMC (ANSMC) scheme for nonlinear systems with uncertainties and external disturbances. However, in these ANSMC techniques, the network weights generally require pretraining. Without proper initialization, the system may oscillate; random or zero-weight initialization can lead to instability or extended convergence time during startup. Overall, these ANSMC approaches rely heavily on the neural network's self-approximation capability. In many cases, expert intervention is required to accelerate convergence and improve approximation accuracy. Therefore, the performance of ANSMC has been further enhanced by incorporating fuzzy logic techniques to exploit expert knowledge and the neural network's adaptive learning capability [27–29], thereby improving adaptability to complex and time-varying uncertainties. However, these controllers typically involve high computational loads, which may hinder their applicability in real-time industrial implementations.

In recent years, terminal SMC techniques have been widely adopted to accelerate convergence within a finite time. Initially, adaptive fuzzy-neural methods [30–32] were combined with terminal SMC to guarantee finite-time convergence under parameter variations and external disturbances. Adaptive fuzzy-neural SMC methods optimize network structures online by combining self-organizing mechanisms with terminal SMC [33], ensuring finite-time convergence. Nevertheless, these controllers impose high computational burdens and have not yet been validated for real-time control applications. Adaptive fuzzy neuro SMC methods [34–36] are combined with nonsingular terminal SMC to eliminate singularities inherent in conventional terminal SMC and ensure fixed-time convergence. This combination also reduces chattering, thereby improving responsiveness to dynamic uncertainties, input saturation, and external perturbations. However, Refs. [34, 35] only verify their results through simulation and do not assess real-time performance. Ref. [36] included both simulation and experimental validation. However, its controller combined multiple techniques, requiring real-time updates of numerous adaptive coefficients, which increases computational cost and limits its applicability to industrial controllers with constrained resources. Refs. [37, 38] propose combining adaptive fuzzy neural networks with super-twisting SMC to reduce chattering further. However, these networks also incur high computational complexity, which imposes significant real-time processing burdens on resource-limited hardware platforms.

Other adaptive fuzzy-neuro SMC approaches utilize RBFNNs to leverage their fast approximation and compensation capabilities for unknown system uncertainties and external disturbances, thereby enhancing control quality [39–41]. Nevertheless, control performance is highly sensitive to the RBFNN parameters. Ref. [41] employed a K-means clustering algorithm to optimize the centers and widths of the RBF neurons. Furthermore, the number and spatial distribution of RBF neurons significantly impact the network's approximation

accuracy, computational load, and responsiveness of the controller. Therefore, these parameters must be carefully optimized in accordance with the control objectives.

Overall, the above analysis indicates that adaptive neural SMC, utilizing RBFNNs and integrated with fuzzy logic, can significantly enhance control performance, robustness, and convergence speed for nonlinear uncertain systems. However, to the best of the authors' knowledge, no existing study has applied an adaptive fuzzy mechanism to tune the stability coefficient of the SMC component within an adaptive neural SMC structure and experimentally validated it on a real CTS. Accordingly, this study proposes a Novel Adaptive Neural Fuzzy Sliding Mode Controller (NANFSMC) for liquid-level regulation in a CTS. The proposed controller addresses the challenges of improving convergence speed and maintaining robustness under uncertain conditions, with stability guaranteed via Lyapunov theory. The proposed method is experimentally validated and compared with the ANSMC and a conventional PID controller [10], which serves as a widely used model-free benchmark.

The main contributions of this paper are summarized as follows:

(1) Novel controller design: development of a NANFSMC for nonlinear uncertain systems regarding sensor perturbation, external disturbances, varying reference signals, and significant time delays. The closed-loop stability of the proposed control system is rigorously guaranteed through a sliding mode control component and an adaptive law, both of which are implemented using the Lyapunov principle. The robustness and convergence speed of the proposed controller are enhanced by combining the adaptive tuning capability of the ANSMC with a TS-fuzzy mechanism that adaptively adjusts the robustness gain of the SMC component. This work provides the first experimental validation of a TS-fuzzy-based adaptive tuning of the robustness gain $\bar{\delta}$ in the SMC component of the proposed controller, implemented on a real CTS under external disturbances.

(2) Computational efficiency and implementability: Adaptive neural fuzzy SMC algorithms generally exhibit high computational complexity, which may hinder real-time implementation on low-cost microcontrollers. Moreover, their numerous parameters complicate controller tuning. To address these limitations, the proposed controller features a simplified structure with a low computational load and a small number of tunable parameters. This design facilitates real-time implementation on low-resource microcontrollers and also extends the controller's applicability to other nonlinear systems, particularly Multi-Input Multi-Output (MIMO) systems.

(3) Improved initialization strategy: Neural network-based controllers typically adopt one of three initialization strategies: (1) Pretrained weights, which require time-consuming selection and may cause significant transient overshoot or instability under real-time uncertainties; (2) Random initialization, which can lead to instability or long convergence time during startup; and (3) Zero-weight initialization, which is simple and easily applied to various systems but may result in slow convergence. To overcome these limitations, this study adopts zero-weight initialization but sets a significant adaptive learning rate during the first 11 s to accelerate convergence. Subsequently, the rate is decreased, and the adaptive fuzzy controller is activated to update the SMC robustness gain. This mechanism rapidly compensates for approximation errors, resulting in rapid stabilization while minimizing overshoot and undershoot as the output error decreases.

The remainder of this study is organized as follows: Section II adequately describes the CTS plant along with the problem formulation. Section III fully presents the design and the implementation of the proposed NANFSMC control algorithm. Section IV analytically presents the experimental results through critical case-studies. Section V eventually concludes the paper.

II. CTS Plant Model and Problem Formulation

Fig. 1 illustrates the two-degree-of-freedom uncertain nonlinear CTS model, based on the Quanser tank model. This CTS model is a part of the quadruple-tank MIMO system depicted in Fig. 2. The CTS system in Fig. 1 consists of a pump with a control voltage u, which pumps liquid into Tank 1, while Tank 2 receives liquid through the outlet pipe of Tank 1. The mathematical model of the CTS plant in Ref. [16] is as in Eq. (1):

$$\begin{cases} \dot{x}_1 = \frac{1}{A_1}(K_p u - b_1 C_1 \sqrt{2gx_1}) \\ \dot{x}_2 = \frac{1}{A_2}(b_1 C_1 \sqrt{2gx_1} - b_2 C_2 \sqrt{2gx_2}) \end{cases} \quad (1)$$

where x_1 and x_2 are the liquid levels in Tank 1 and 2; u is the control voltage for the pump's motor, serving as the system input. The system output can be x_1, x_2 or both x_1 and x_2. The control objective aims to regulate the liquid level in Tank 1, Tank 2, or both, tracking the desired liquid level. This paper focuses on controlling the liquid level in Tank 2. The physical values of the model parameters are presented in Table I for reference. Due to the small tank area, the output sensor exhibits high noise, as it is significantly affected by the outflow from the pump and the drainage from the upper tank. This poses a significant challenge for controlling this system.

In the experimental setup, the physical parameters listed in Table I can be approximately measured, except for the discharge coefficients C_1 and C_2, which cannot be obtained through conventional measurement methods and are therefore assumed to be unknown. Consequently, the controller must be capable of approximating all parameters presented in Table I.

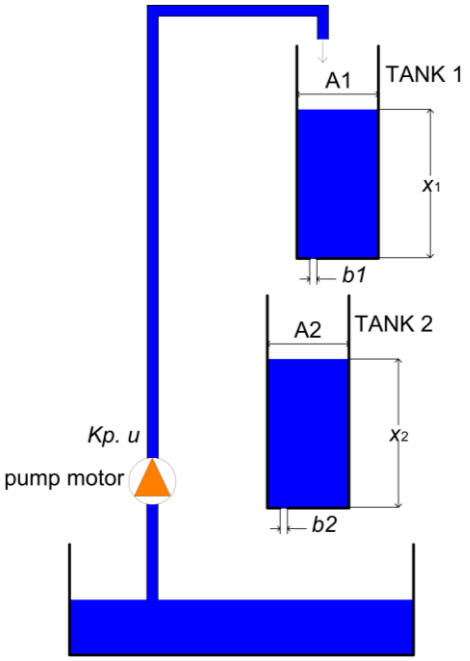

Fig. 1. Coupled Tank System (CTS).

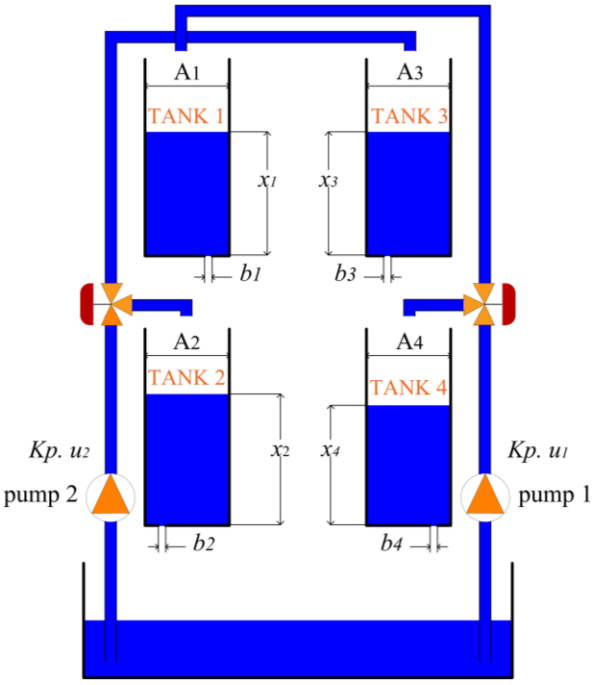

Fig. 2. Quadruple-Tank System (QTS).

TABLE I. COUPLED-TANK SYSTEM PARAMETERS FOR REFERENCE

Symbol	Explanation	Size	Unit
A_1	Inner surface area of Tank 1	16.619	cm^2
A_2	Inner surface area of Tank 2	16.619	cm^2
b_1	Drainpipe area in Tank 1	0.5	cm^2
b_2	Drainpipe area in Tank 2	0.33	cm^2
C_1	Discharge coefficient at the outlet of Tank 1	-	-
C_2	Discharge coefficient at the outlet of Tank 2	-	-
g	Gravitation force	981	cm/s^2
K_p	Gain of the pump	10.42	$cm^3/s/V$

Next is the design of the proposed NANFSMC controller for the CTS system Eq. (1).

$$\begin{cases} \dot{x} = f(x) + g(u) \\ y = h(x) \end{cases} \tag{2}$$

Let $h(x) = x_2$, rewrite Eq. (2) as Eq. (3):

$$\begin{cases} \dot{x}_1 = \frac{1}{A_1}(K_p u - b_1 C_1 \sqrt{2gx_1}) \\ \dot{x}_2 = \frac{1}{A_2}(b_1 C_1 \sqrt{2gx_1} - b_2 C_2 \sqrt{2gx_2}) \\ y = x_2 \end{cases} \tag{3}$$

The CST system Eq. (1) can be rewritten as Eq. (4):

$$\ddot{y} = a(x) + b(x)u \tag{4}$$

The purpose of control is to track output $y(t)$ according to the desired value $y_d(t)$. Eq. (4) can be rewritten as Eq. (5):

$$u = \frac{1}{b(x)}[-a(x) + v(t)] \tag{5}$$

If both nonlinear descriptions $a(x)$ and $b(x)$ represent known a priori, the ideal control law given in Eq. (5) can be directly computed. However, these functions are typically unknown in practical control applications or may vary over time due to changes in parameters and variations in operating conditions. Consequently, direct implementation of the ideal control law Eq. (5) is generally infeasible. In the case where $a(x)$ and $b(x)$ seem undetermined, the problem reduces to designing a control law that can accurately approximate the ideal controller in real-time. To this end, this paper introduces a NANFSMC, an online approximation of the ideal control law Eq. (5) for water-level regulation in the CTS. The detailed formulation and design procedure of the proposed approach will be fully introduced in the following section.

III. DESIGN THE PROPOSED NANFSMC CONTROL ALGORITHM

A. The Proposed NANFSMC Algorithm for the Coupled-Tank Plant

Fig. 3 illustrates the structure of the proposed NANFSMC for the CTS plant, which comprises an adaptive control component and an SMC component. Where the SMC parameters are updated in real-time by the adaptive fuzzy controller. The ideal controller Eq. (5) is estimated by the adaptive controller using an RBFNN with two inputs, e_2 and $\dot{e}_2$, fifteen RBF neurons in the hidden layer, and one output $\hat{u}$ as shown in Fig. 4.

The adaptive controller is computed based on the structure shown in Fig. 4 and defined in Eq. (6),

$$\hat{u} = h^T w \tag{6}$$

The output of the hidden layer is denoted by h function as presented in Eq. (7):

$$h(x) = [h_1(x)\ h_2(x) \dots h_{15}(x)]^T \tag{7}$$

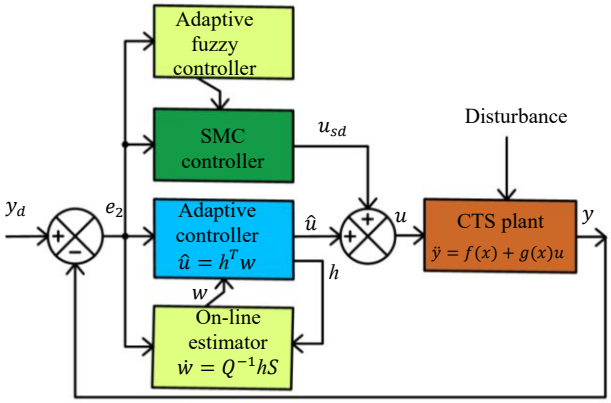

Fig. 3. Layout of the proposed NANFSMC controller.

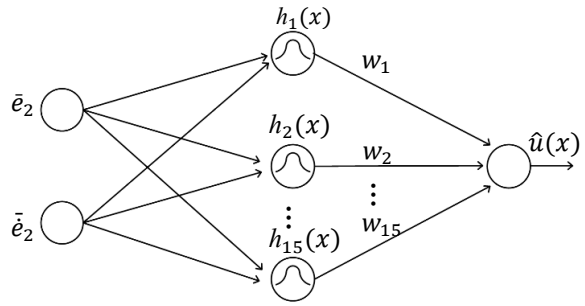

Fig. 4. Approximation of the linearized feedback controller using the RBFNN.

The activation function of the *i*-th RBF neuron is as in Eq. (8):

$$h_i(x) = e^{-\frac{\left[(\bar{e}_2 - c_{1i})^2 + (\dot{\bar{e}}_2 - c_{2i})^2\right]}{2\rho_i^2}} \tag{8}$$

The dispersions ρ_i ($i = 1,\ldots,15$) are selected to be equal, and these functions are selected to distribute uniformly throughout the state space; select $\rho_i = \rho$. Fig. 5 displays the distribution of the RBF neuron centers' locations.

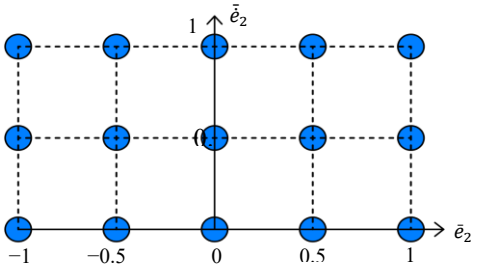

Fig. 5. Center placements of the RBFNN.

The values of the signals $\bar{e}_2$ and $\dot{\bar{e}}_2$, corresponding to the feedback signals e_2 and $\dot{e}_2$ given back to the controller, they are normalized to stay within the range [0, 1].

Based on the limited physical magnitudes of e_2 and $\dot{e}_2$, this paper selects $ke_2 = 1/30$ and $k\dot{e}_2 = 1/30$. The weight vector of the RBFNN's output layer is denoted by *w* as illustrated in Eq. (9):

$$w = [w_1\ w_2\ \ldots\ w_{15}]^T \tag{9}$$

To bring $\hat{u}$ closer to the ideal value u^*, the RBFNN updates the vector w online. The network has a structural error $\delta(x)$ since it uses a limited number of RBF neurons in the hidden layer to approximate the optimal control law as described in Eq. (10):

$$u^*(x) = w^* h(x) + \delta(x) \tag{10}$$

As a result, the difference in the optimal control rule, u^*, with the achieved rule, $\hat{u}$, is shown below in Eq. (11).

$$\hat{u}(x) - u^*(x) = \tilde{w}h(x) - \delta(x) \tag{11}$$

with $\tilde{w}$ stands for the approximation error shown in Eq. (12).

$$\tilde{w} = w - w^* \tag{12}$$

Assumption 1: Since the RBFNN approximates the controller in a way that makes it possible to know the upper bound of the structural error $\delta(x)$ in advance, there is a continuous function $\bar{\delta}(x)$ such that $|\delta(x)| \leq \bar{\delta}(x), \forall x$.

We choose the following control law as presented in Eq. (13) to ensure the stability of the system because of the structural error $\delta(x)$.

$$u = \hat{u} + u_{sd} \tag{13}$$

where the sliding mode controller u_{sd} stabilizes the system and is selected so that the derivative of the Lyapunov function is negative semi-definite. Eq. (4) gives us the following Eq. (14).

$$\begin{aligned} \ddot{y} &= a(x) + b(x)u^*(t) + b(x)[u(t) - u^*(t)] \\ \ddot{y} &= v(t) + b(x)[u(t) - u^*(t)] \end{aligned} \tag{14}$$

In which $v(t) \in R$, and is defined as in Eq. (15),

$$v(t) = \ddot{y}_d + \bar{S} + k_1 S \tag{15}$$

With $k_1 > 0$, the definitions that follow provide S and $\bar{S}$ as presented in Eqs. (16)–(18):

$$S(t) = \dot{\bar{e}}_2(t) + k_1 \bar{e}_2(t) \tag{16}$$

$$e_2(t) = y_d(t) - y(t) \tag{17}$$

$$\bar{S} = \dot{S} - \dot{\bar{e}}_2 \tag{18}$$

where the sliding surface is denoted by $S(t)$ and the plant's output error by $e_2(t)$. Here, the Routh-Hurwitz stability criterion is satisfied by the choice of parameter k_1.

Combining Eqs. (14), (15), and (18) results in Eq. (19) and induced to Eqs. (20) and (21):

$$\dot{\bar{e}}_2(t) = \ddot{y}_d(t) - \ddot{y}(t) \tag{19}$$

$$\ddot{\bar{e}}_2(t) = \ddot{y}_d(t) - v(t) - b(x)[u(t) - u^*(t)] \quad (20)$$

$$\ddot{\bar{e}}_2(t) = -\dot{\bar{S}} - k_1 S - b(x)[\hat{u}(t) + u_{sd}(t) - u^*(t)] \quad (21)$$

Here, Eq. (11) and (18) are substituted into Eq. (21), then the nonlinear features of the residual are described in Eq. (22):

$$\dot{S} + k_1 S = -b\tilde{w}h(x) + b\delta(x) - bu_{sd} \quad (22)$$

Choosing a Lyapunov function that is quadratic as presented in Eq. (23):

$$V = \frac{1}{2b}S^2 + \frac{1}{2}\tilde{w}^T Q\tilde{w} \quad (23)$$

where Q is a positive constant.

Assumption 2: $b(x)$ stays inside a defined range as follows,

$$0 < \underline{b}(x) \le b(x) \le \bar{b}(x) < \infty$$

Since Eq. (23) is differentiated with respect to time, Eq. (24) is determined as,

$$\dot{V} = \frac{1}{b}S\dot{S} - \frac{\dot{b}}{2b^2}S^2 + \tilde{w}^T Q\dot{w} \quad (24)$$

Upon inserting Eq. (22) into Eq. (24), we get Eq. (25):

$$\dot{V} = -\frac{k_1 S^2}{b} - Su_{sd} + S\delta + \tilde{w}^T(Q\dot{w} - hS) - \frac{\dot{b}}{2b^2}S^2 \quad (25)$$

Then the adaptive law selection is as Eq. (26).

$$\dot{w} = Q^{-1}hS \quad (26)$$

During the control process, the output weights of the RBFNN are updated according to Eq. (26) to eliminate the RBFNN approximation error $\tilde{w}$ in Eq. (25). This updating mechanism helps drive the sliding surface S to converge to 0. However, due to the structural error $\bar{\delta}$ defined in Eq. (10), which always exists during the approximation process because of the finite number of RBF neurons. As a result, the sliding surface S may not converge to 0 even when the approximation error is canceled. Moreover, this structural error can potentially cause system instability. Therefore, to ensure system stability and convergence, an additional SMC control term is introduced as follows.

Putting Eq. (26) into Eq. (25), we obtain Eq. (27),

$$\begin{aligned} \dot{V} &= -\frac{k_1 S^2}{b} - Su_{sd} + S\delta - \frac{\dot{b}}{2b^2}S^2 \\ \dot{V} &\le -\frac{k_1 S^2}{b} - Su_{sd} + |S|(|\delta| + \frac{|\dot{b}|}{2b^2}|S|) \\ \dot{V} &\le -\frac{k_1 S^2}{\bar{b}} - Su_{sd} + |S|(\bar{\delta} + \frac{\gamma}{2\underline{b}^2}|S|) \end{aligned} \quad (27)$$

Assumption 3: There is a continuous function $\gamma(x)$ for which $|\dot{b}|(x) \le \gamma(x)$, and $b(x)$ has a limited fluctuation rate.

Choose the sliding mode controller as presented in Eq. (28):

$$u_{sd} = (\bar{\delta} + \frac{\gamma}{2\underline{b}^2}|S|)\, sgn(S) \quad (28)$$

Substituting Eq. (28) into Eq. (27), we obtain Eq. (29):

$$\dot{V} \le -\frac{k_1 S^2}{\bar{b}} \le 0 \quad (29)$$

The positive definite quadratic function V has $\dot{V} \le 0$. Therefore, the proposed NANFSMC ensures the stability of system operation.

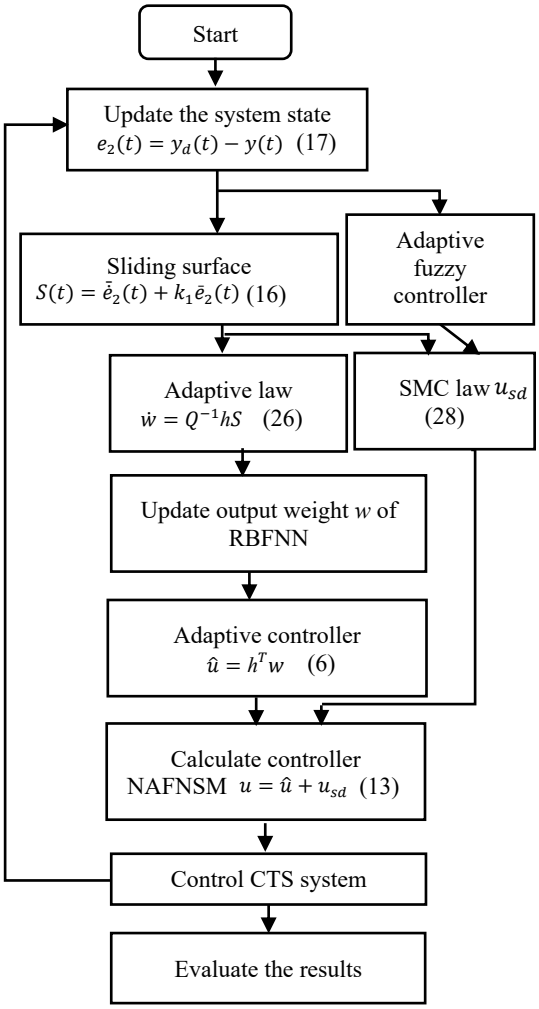

Fig. 6. The proposed NANFSMC Controller flowchart.

The overall operating principle of the proposed NANFSMC controller is illustrated in the flowchart shown in Fig. 6. At the beginning of operation, the system states $e_2(t)$ are updated. The tracking error $e_2(t)$ and its derivative $\dot{\bar{e}}_2$ are normalized to the range [0,1] and then used to compute the sliding surface (16), the adaptive law Eq. (26), and the SMC law Eq. (28). The output weights w in the adaptive controller Eq. (6) are updated online by the

RBFNN. Simultaneously, based on the current error, the stability gain in the SMC controller Eq. (28) is also updated online through the adaptive fuzzy controller. Then, the total control signal, as described in Eq. (13), is calculated. Finally, the control performance of the proposed algorithm is evaluated.

B. *The Adaptive Fuzzy Controllers in the Proposed NANFSMC Controller*

In the SMC controller given by u_{sd} Eq. (28), the gain $\bar{\delta}$ functions analogously to the stability gain K in conventional SMC schemes. Selecting a large value for this gain results in faster stabilization but may cause significant overshoot and undershoot in the output response when the reference signal changes or disturbances occur. Conversely, selecting a small gain reduces overshoot and undershoot, but slows the system's response and decreases its robustness against reference variations, model uncertainties, and, in particular, external disturbances. To exploit the advantages and mitigate the drawbacks associated with this gain, this paper proposes an adaptive fuzzy controller (Fig. 7) based on the Takagi-Sugeno fuzzy inference system to adaptively tune the gain $\bar{\delta}$ in real time. This adaptive mechanism enhances both the transient response and robustness of the SMC controller in Eq. (28), while maintaining low overshoot and undershoot under all aforementioned uncertainties. Consequently, the overall performance of the NANFSMC is satisfactorily ameliorated.

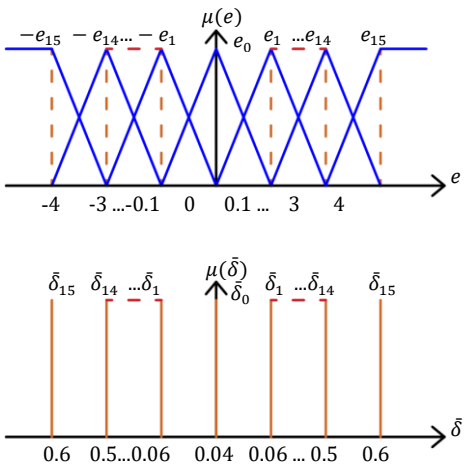

Fig. 7. Input and output of the adaptive fuzzy controller.

The fuzzy MF inputs and output, illustrated in Fig. 7, consist of a single input e and a single output $\bar{\delta}$, where e represents the error values before normalization to the range [0, 1]. These values are selected as: $[e_0, e_1, \ldots e_{14}, e_{15}]$ = [0, 0.1, 0.15, 0.2, 0.25, 0.3, 0.35, 0.4, 0.6, 0.8, 1.2, 1.6, 2, 2.5, 3, 4]; $[\bar{\delta}_0, \bar{\delta}_1, \ldots \bar{\delta}_{14}, \bar{\delta}_{15}]$ = [0.04, 0.06, 0.08, 0.1, 0.2, 0.23, 0.24, 0.25, 0.26, 0.3, 0.34, 0.38, 0.42, 0.46, 0.5, 0.6].

A TS fuzzy model is employed, in which the input membership functions are triangular and trapezoidal, while the output membership function is the singleton type. The fuzzy rule base follows the general form: If $e_i = \alpha$ then, $\bar{\delta}_i = \beta$, where α and β are fuzzy sets. The fuzzy inference mechanism employs the MAX–MIN composition, and the defuzzification method is the Sugeno weighted-average approach, as expressed below in Eq. (30):

$$\bar{\delta} = \frac{\sum_{i=1}^{15} \bar{\delta}_i \mu(\bar{\delta}_i)}{\sum_{i=1}^{15} \mu(\bar{\delta}_i)} \tag{30}$$

with $\mu(\bar{\delta}_i)$ is the firing strength of the i^{th} fuzzy rule.

The operating principle of the proposed adaptive fuzzy controller is straightforward yet effective. When the input e increases, the output $\bar{\delta}$ is adaptively increased to accelerate the system response. Conversely, when e decreases, $\bar{\delta}$ is reduced to suppress overshoot and undershoot. As $\bar{\delta}$ is minimized while still maintaining sufficient robustness to reject output sensor noise and actuator uncertainties in the pump motor. This mechanism enables the proposed NANFSMC to achieve smoother responses, faster transient performance, and higher stability compared to the conventional ANSMC with a fixed $\bar{\delta}$ gain. The effectiveness of this approach is demonstrated through experimental results presented in the following section.

IV. Experiment Validation

The response quality of the proposed controller and the PID control method is evaluated on a real-time control algorithm for the CTS system. The procedure for real-time validation is outlined in Fig. 8. The experimental setup, shown in Fig. 9, consists of a central control board based on the TMS320F28379D microcontroller, a sensor signal amplifier for the MPX10 sensor, a PWM modulation unit, a JT-750 pump (24 VDC), and a laptop running Matlab/Simulink 2023b with the "Monitor & Tune" tool for real-time monitoring and data visualization.

The sensor feedback signal is passed through the Sensor Signal Amplifier before being sent to the Central Control Board. The data from this board is transmitted and displayed on the PC via SCI communication.

Real-time validation is conducted through two benchmark scenarios. The first benchmark evaluates the system's output response to a multi-level reference signal comprising three step-up transitions and one step-down transition, as described in Ref. [9]. The second benchmark assesses performance under significant external disturbances. Both benchmarks are applied consistently to all three controllers: the proposed NANFSMC, ANSMC, and PID control method described in Ref. [8]. The PID controller in Ref. [8] is reformulated for the CTS model as presented in Eq.(31):

$$u_{PID}(t) = k_p e_2(t) + k_i \int_0^t e_2(t)dt + k_d \dot{e}_2(t) \tag{31}$$

The PID parameters can be tuned through trial and error, as performed in Ref. [9] for multiple test cases. However, since the present study focuses primarily on step responses, such tuning would not fully reflect the controller's performance under varying reference signals.

Therefore, in this work, the PID parameters are selected based on their performance in tracking a time-varying reference signal. The response quality corresponding to each parameter set is evaluated using error-based performance indices, and the parameter set yielding the best performance is chosen for comparison with the proposed control algorithm.

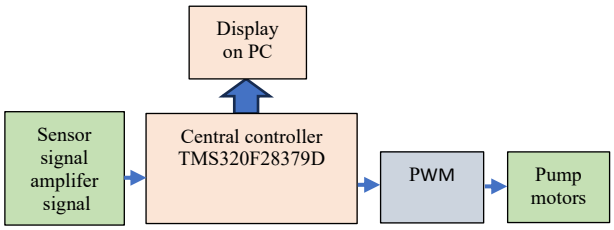

Fig. 8. Diagram of the real-time experimental setup.

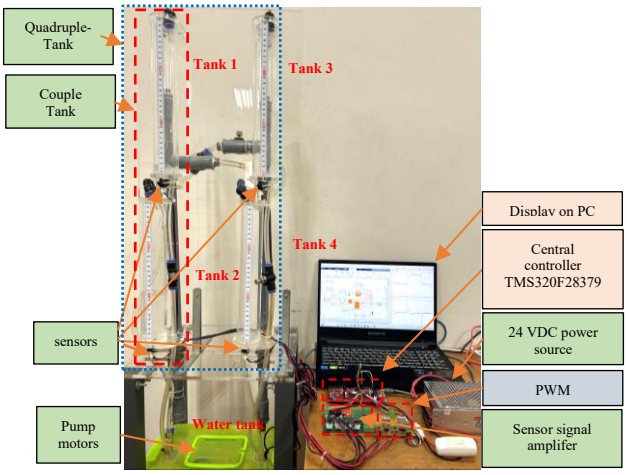

Fig. 9. Real-time validation arrangement.

TABLE II. TUNING PARAMETERS OF THE PID CONTROLLER FOR DIFFERENT TEST CASES

Parameters	Case 1	Case 2	Case 3	Case 4	Case 5	Case 6	Case 7
k_p	1	1.1	0.9	1	1	1	1
k_i	0.0458	0.0458	0.0458	0.0458	0.0458	0.0448	0.0468
k_d	1.2	1.2	1.2	1.3	1.1	1.2	1.2

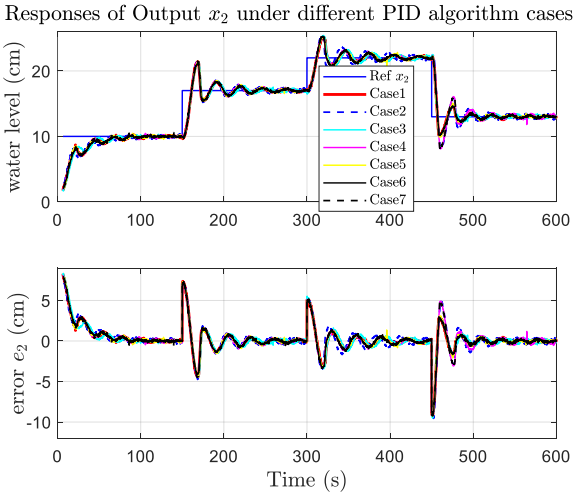

Fig. 10. Comparative results of CTS output responses for different PID controller parameter test cases.

The PID controller parameters are tuned for multiple test cases, with seven representative cases presented in Table II. The corresponding output responses of the CTS for these seven parameter sets are shown in Fig. 10.

Table III presents the output performance of the CTS for the seven parameter test cases corresponding to the parameter sets listed in Table II. The results indicate that Case 1 yields the best response quality among all cases. Therefore, the parameters of Case 1 are selected for comparison with the proposed NANFSMC in the subsequent analysis.

Next, the parameter selection for the proposed controller and the ANSMC is discussed. The parameters of both controllers are chosen to achieve a trade-off among fast transient response, minimal overshoot and undershoot, and the lowest possible steady-state error, while ensuring stability under sensor noise, pump uncertainties inherent in real-time control, and external disturbances. In both algorithms, the output weights w of the RBFNNs in the adaptive controller Eq. (6) are initialized to 0, eliminating the need for pre-optimized weight initialization. Instead, both controllers are initialized with higher adaptation gains during the startup phase, specifically $Q_0^{-1} = 0.046$ for the first 11 s, to accelerate the initial adaptation of the RBFNNs. This gain is then reduced to 0.012 to suppress overshoot and undershoot when the reference signal changes. In addition, the gain $\bar{\delta} = 0.3$ of the SMC controller in Eq. (28) is fixed at 0.3 for the first 11 s. Subsequently, in the proposed controller, this gain is adaptively updated in real-time by the adaptive fuzzy controller described in Section III, whereas in the ANSMC, it remains constant $\bar{\delta} = 0.1$. The control performance of the algorithms is evaluated using error-based performance indices, namely the Integral of Absolute Error (IAE), Mean Absolute Error (MAE), and Integral of Time-weighted Absolute Error (ITAE). The remaining parameters— ρ^2 in Eq. (8) and k_1 in Eq. (16)—are set identically for both the proposed controller and the ANSMC: $\rho^2 = 0.35$, $k_1 = 0.1$.

TABLE III. PERFORMANCE METRICS OF THE PID CONTROLLER FOR DIFFERENT PARAMETER TEST CASES

Criterion	Case 1	Case 2	Case 3	Case 4	Case 5	Case 6	Case 7
IAE	478.467	572.071	509.696	534.829	481.773	485.603	504.112
MAE	0.808	0.966	0.861	0.903	0.814	0.820	0.852
ITAE	2.832×10^6	3.386×10^6	3.017×10^6	3.166×10^6	2.852×10^6	2.874×10^6	2.984×10^6

A. The First Benchmark Test

The first benchmark verifies the system's output response to a multi-level reference signal consisting of three step-up transitions and one step-down transition, specifically from 10 cm to 17 cm, then to 22 cm, and finally decreasing to 13 cm, as described in Ref. [9]. This test is used to evaluate and compare the response quality of the control algorithms.

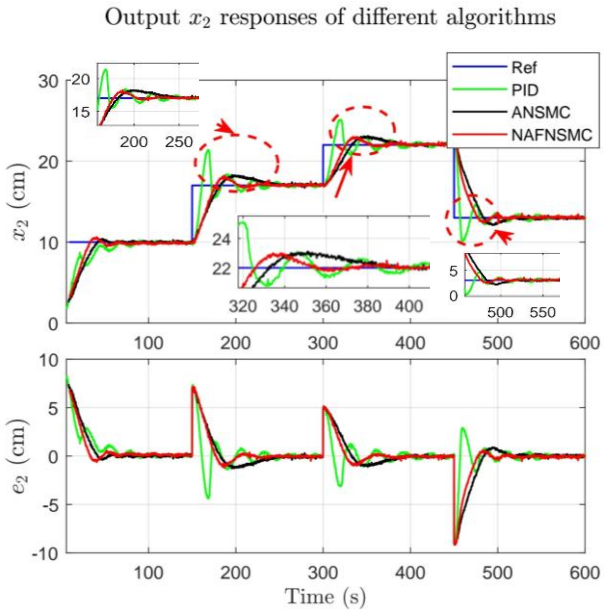

Fig. 11. Comparison of CTS output responses obtained with the proposed NANFSMC, the ANSMC, and the PID controller under varying reference signals.

Fig. 11 shows that all controllers generally track the reference signal effectively. The PID controller exhibits a slower startup than the other methods, reaching steady state after approximately 100 s, but with negligible overshoot and undershoot during the initial rise. However, when the reference signal changes, the PID controller responds faster but produces significantly higher overshoot and undershoot. In contrast, both the proposed NANFSMC and the ANSMC achieve significantly lower overshoot and undershoot compared to the PID controller. Specifically, when the reference signal increases from 10 cm to 17 cm, the PID controller exhibits an overshoot of approximately 21.4 cm and an undershoot of 15.5 cm, reaching the steady state after about 100 s. The proposed controller limits overshoot to 18 cm, eliminates undershoot, and achieves a steady state in approximately 50 s. The ANSMC also limits overshoot to 18 cm, with no undershoot, but settles more slowly, at around 90 s. When the reference signal rises to 22 cm, the PID controller produces an overshoot of 25 cm, an undershoot of 20.8 cm, and reaches a steady state after approximately 100 s. The proposed controller limits overshoot to 23 cm, with no undershoot, achieves a settling time of 52 s. In comparison, the ANSMC also limits overshoot to 23 cm, with no undershoot, but requires approximately 82 s to reach a stable state. Finally, when the reference signal decreases sharply from 22 cm to 13 cm, the PID controller exhibits an undershoot of approximately 10 cm, an overshoot of 14.5 cm, and settles after more than 100 s. The proposed controller reduces the undershoot to approximately 12.5 cm, exhibits almost no overshoot, and settles in about 40 s. The ANSMC yields a slightly larger undershoot of 12.1 cm, no overshoot, and settles more slowly at around 60 s. These results demonstrate that under varying reference signals, the proposed controller achieves significantly lower overshoot and undershoot and reaches the steady state more quickly than the ANSMC and PID controllers. Furthermore, the error-based performance indices summarized in Table IV show improvements of up to 23.8% and 7.8% in the IAE and MAE indices compared to the ANSMC and PID controllers, respectively. These results demonstrate that the proposed controller achieves a faster transient response and reaches the steady state more quickly than the other two algorithms.

TABLE IV. COMPARISON OF TOTAL ERROR-BASED PERFORMANCE INDICES FOR OUTPUT RESPONSES UNDER VARYING REFERENCE SIGNALS

Criterion	NANFSMC	ANSMC	PID
IAE	444.0404	582.5631	478.4671
MAE	0.7518	0.9864	0.8101
ITAE	2.6225×10^6	3.4406×10^6	2.8258×10^6

B. The Second Benchmark Test

Validation is further performed with a multi-level reference signal in the presence of external disturbances applied at two time instants: 300 s and 500 s, corresponding to reference levels of 17 cm and 20 cm, respectively. These disturbances are introduced by adding water volume equivalent to a height of 7 cm in the tank, corresponding to abrupt increases of approximately 35% and 41% of the respective reference levels.

Fig. 12 compares the CTS output responses of the three controllers—proposed NANFSMC, ANSMC, and PID—under varying reference signals, external disturbances, and sensor noise. When a disturbance is applied at t = 300 s with the reference signal at 17 cm, the PID controller produces a fast response but with a significant overshoot of approximately 19.6 cm and a large undershoot of about 12.2 cm, followed by sustained oscillations around the reference and a recovery time exceeding 100 s. The proposed controller eliminates overshoot, limits undershoot to approximately 16.1 cm, and achieves recovery in about 48 s. The ANSMC also achieves 0 overshoot and slightly higher undershoot at 15.9 cm, but settles more slowly, requiring approximately 75 s. When a disturbance is applied at t = 500 s with the reference at 20 cm, the PID controller again produces a fast initial response but exhibits an overshoot of approximately 21.4 cm, an undershoot of 17.0 cm, and oscillations that persist for exceeding 100 s before recovery. The proposed controller eliminates overshoot, limits undershoot to about 19 cm, and recovers within 52 s. The ANSMC achieves 0 overshoot, an undershoot of 18 cm, and a slower recovery time of approximately 82 s. These experimental results demonstrate that the proposed NANFSMC and the ANSMC maintain stable operation under significant external disturbances, with the proposed controller consistently achieving substantially faster recovery times

than the ANSMC and PID controllers. In contrast, the PID controller exhibits significant overshoot and undershoot values, as well as prolonged oscillations, before returning to its steady state. Furthermore, the error-based performance indices summarized in Table V show improvements of up to 22.9% and 14.2% in the IAE and MAE indices compared to the ANSMC and PID controllers, respectively. The percentage improvement over the PID controller increases from 7.8% in the first benchmark test to 14.2% in the second benchmark test, indicating that the proposed controller exhibits enhanced responsiveness and disturbance rejection capability compared to the PID algorithm.

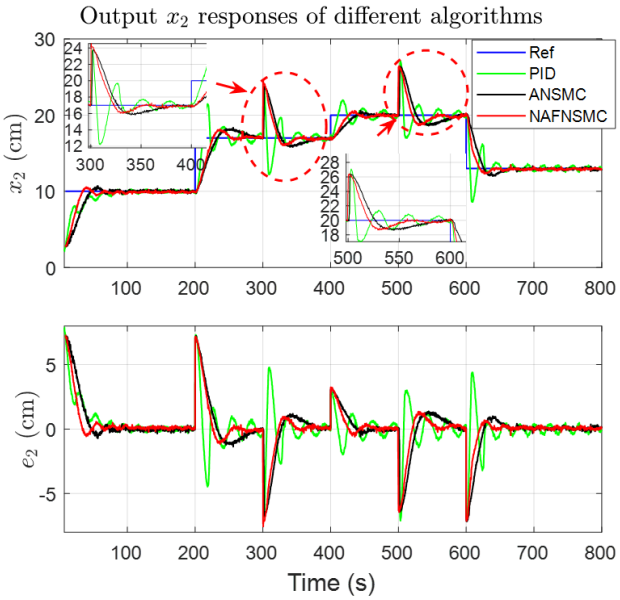

Fig. 12. Comparison of CTS output responses obtained with the proposed NANFSMC, the ANSMC, and the PID controller under varying reference signals, external disturbances, and sensor noise.

TABLE V. COMPARISON OF TOTAL ERROR-BASED PERFORMANCE INDICES FOR OUTPUT RESPONSES UNDER VARYING REFERENCE SIGNALS, EXTERNAL DISTURBANCES, AND SENSOR NOISE

Criterion	NANFSMC	ANSMC	PID
IAE	587.664	761.7629	684.7973
MAE	0.9955	1.2905	1.1601
ITAE	3.469×10^{6}	4.4967×10^{6}	4.0424×10^{6}

Fig. 13 presents the output response along with the real-time updated value of $\bar{\delta}$ in the SMC component of the proposed controller, as adjusted by the fuzzy controller under varying reference signals, external disturbances, and sensor noise. When the error e is large, corresponding to substantial reference signals changes or significant external disturbances, the fuzzy controller increases $\bar{\delta}$ to enable the SMC component to stabilize the system rapidly. This mechanism is clearly illustrated in the zoomed view from 620 s to 660 s, where the reference signal decreases from 20 cm to 13 cm, and the value of $\bar{\delta}$ rapidly increases to approximately 0.23 to quickly suppress the undershoot. Conversely, when the tracking error e becomes small, $\bar{\delta}$ is reduced to generate a smoother response while maintaining stable steady-state operation under the influence of output sensor noise, pump motor uncertainties, and other system disturbances.

This behavior is further confirmed in the zoomed view from 780 s to 800 s, where the ANSMC algorithm exhibits a steady-state error within the range of [−0.3, 0.2] cm, whereas the proposed controller maintains a smaller error within [−0.1, 0.1] cm due to the adaptively updated $\bar{\delta}$ value ranging from 0.04 to 0.07. In contrast, the ANSMC algorithm fixes this parameter at 0.1 to maintain control performance. These results demonstrate that the stability gain in the SMC component of the proposed controller is rapidly updated under all uncertain conditions, enabling the system to achieve faster yet smoother stabilization compared to the ANSMC algorithm.

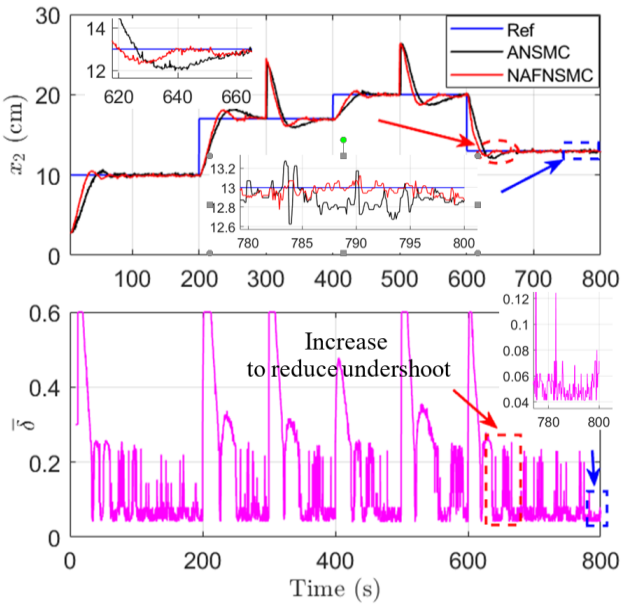

Fig. 13. Output response and adaptively updated value of $\bar{\delta}_i$ by the fuzzy controller in the proposed NANFSMC under varying reference signals, external disturbances, and sensor noise.

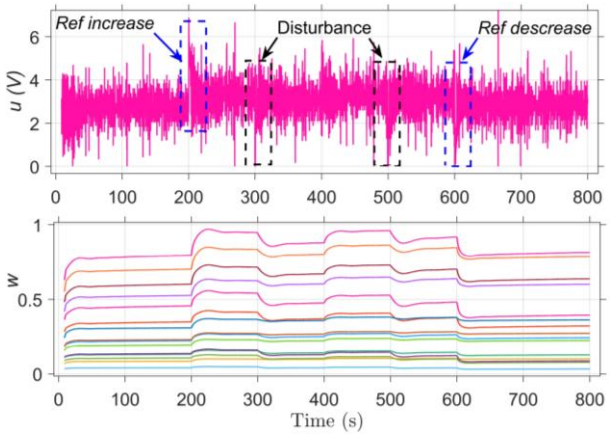

Fig. 14. Control input response and real-time adaptively updated output weights w of the RBFNN in the proposed NANFSMC under varying reference signals, external disturbances, and sensor noise.

Fig. 14 illustrates the real-time adaptive variations of the output weights w of the RBFNN in the proposed NANFSMC, along with the corresponding changes in the

control input, under varying reference signals, external disturbances, and sensor noise. When the reference signal changes or disturbances occur, the values of w exhibit significant variations, enabling the proposed controller to adapt effectively to these changing operating conditions.

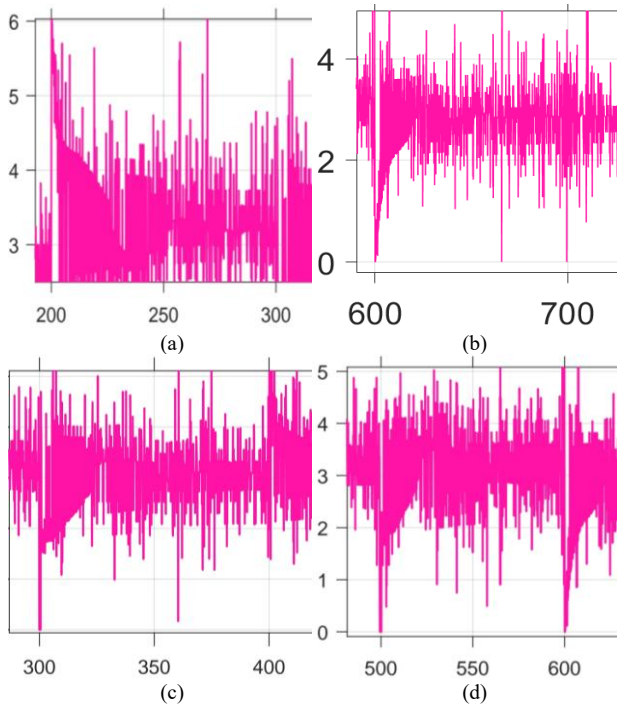

Fig. 15. Zooming control input response and real-time adaptively updated output weights w of the RBFNN in the proposed NANFSMC under varying reference signals, external disturbances, and sensor noise. (a) control signal u increases; (b) control signal u decreases (with reference signal decreases from 22 cm to 13 cm at 600 s); (c) control signal u decreases (with reference level of 17 cm); (d) control signal u decreases (with reference level of 22 cm).

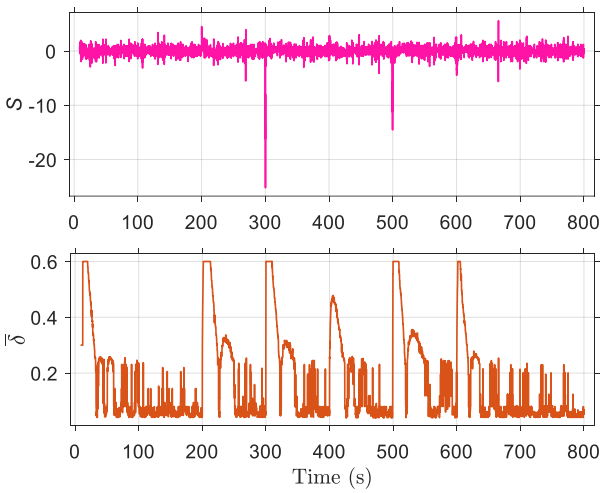

Fig. 16. Adaptively updated values of $\bar{\delta}_i$ corresponding to the convergence of sliding surfaces in the proposed NANFSMC under varying reference signals, external disturbances, and sensor noise.

Fig. 15 presents the zoomed-in view of Fig. 14. In Fig. 15(a), when the reference signal increases from 10 cm to 17 cm at 200 s, the magnitude of the control signal u rises from approximately 3 V to 6 V to drive the pump output to 17 cm and then decreases to around 3.2 V to maintain this new level. Conversely, as shown in Fig. 15(b), when the reference signal decreases from 22 cm to 13 cm at 600 s, the control signal u drops to 0 V and subsequently increases to about 2.8 V to sustain the liquid level at 13 cm. When external disturbances are introduced, the output level rises at 300 s and 500 s in the Fig. 15(c) and (d), respectively, the control signal u quickly drops to 0 V and then rapidly increases to approximately 3.2 V and 3.6 V, corresponding to the reference levels of 17 cm and 22 cm. Additionally, the amplitude of u continuously varies in response to output sensor noise, which is always present in real-time control systems. These results demonstrate that the control signal u rapidly adapts to varying reference signals, external disturbances, and output sensor noise.

In Fig. 16, the value of $\bar{\delta}$ in the SMC controller Eq. (28) is updated in accordance with the convergence of the sliding surfaces S in the proposed NANFSMC under varying reference signals, external disturbances, and sensor noise. When the reference signal changes or when disturbances occur at t = 300 s and t = 500 s, $\bar{\delta}$ increases to enhance stabilization speed. When S becomes small, $\bar{\delta}$ is reduced, resulting in smoother system behavior while maintaining stability. This adaptive adjustment enables the proposed controller to achieve faster responses, higher stability, and smoother performance compared to the ANSMC, which has the value of $\bar{\delta}$ fixed. The experimental results demonstrate that the proposed controller outperforms both the ANSMC and the PID controller in scenarios involving varying reference signals (Fig. 11) and significant external disturbances (Fig. 12). The proposed controller delivers fast responses with low overshoot and undershoot. While the ANSMC also achieves low overshoot and undershoot, it exhibits slower settling than the proposed method. The PID controller responds quickly but suffers significant overshoot, large undershoot, and sustained oscillations. Furthermore, the performance indices in Tables IV and V confirm that the proposed controller achieves superior results across all evaluated metrics. In addition, Figs. 13–16 illustrate the online adaptation capability of the RBFNN output weights w in the adaptive controller Eq. (6) and the parameter $\bar{\delta}$ in the SMC controller Eq. (28) under varying reference signals, external disturbances, and output sensor noise. These adaptive mechanisms enable the proposed controller to respond faster, maintain robustness, and produce smoother control actions compared to both the ANSMC and the PID controller. This validates the effectiveness of integrating ANSMC with the fuzzy logic technique to enhance control performance.

V. Conclusion

This paper presents a NANFSMC to control uncertain nonlinear systems with unknown dynamic models. The proposed controller integrates two components: (1) an adaptive control component, approximated by an RBFNN, and (2) an SMC component for system stabilization. The adaptation and SMC laws are derived using Lyapunov stability theory. In the proposed scheme, the parameter of

the SMC component is updated in real-time by an adaptive fuzzy controller, thereby improving the transient response speed and overall control quality.

The efficiency of the proposed NANFSMC is experimentally verified on a CTS under various test scenarios, with its performance compared to that of the ANSMC and PID controllers. This is the first experimental validation of a TS-fuzzy–tuned SMC robustness gain implemented on a real CTS under external disturbances, achieving improvements of up to 22.9% and 14.2% in the IAE, MAE, and ITAE indices compared to the ANSMC and PID controllers, respectively. These results verify that the proposed controller possesses a strong ability to maintain system stability under varying reference signals, sensor noise, and, particularly, significant external disturbances.

Furthermore, the proposed controller features a simple structure with low computational load and a small number of tuning parameters, making it easily applicable to other nonlinear systems, especially nonlinear MIMO processes. In addition, although the RBFNN output weights are initialized to 0, thus eliminating the need for pre-optimized weight selection, the system still exhibits fast convergence with minimal overshoot and undershoot. This performance is achieved through the integration of an adaptive fuzzy mechanism, which dynamically adjusts the stability gain of the SMC component to rapidly compensate for the approximation error of the RBFNN in the neural adaptive controller. As a result, the system stabilizes quickly while minimizing overshoot and undershoot at low levels as the output error decreases.

However, although the controller is designed for simplicity and computational efficiency, it has not yet been experimentally verified on nonlinear MIMO systems. Therefore, future work will focus on extending the proposed control strategy to nonlinear MIMO processes to evaluate its scalability and computational performance.

Conflict of Interest

The authors declare no conflict of interest.

Author Contributions

NAT: theory, writing-original draft, supervision, reviewing, software coding; HPHA: methodology, editing; all authors had approved the final version.

Acknowledgment

We acknowledge Ho Chi Minh City University of Technology (HCMUT), VNU-HCM, for supporting this study.

References

[1] U. M. Nath, C. Dey, and R. K. Mudi, "Desired characteristic equation based PID controller tuning for lag-dominating processes with real-time realization on level control system," *IEEE Control Syst. Lett.*, vol. 5, no. 4, pp. 1255–1260, 2021.

[2] M. N. Kamarudin, S. M. Rozali, S. N. M. Azam *et al.,* "Formulation of a Lyapunov-based PID controller for level control of a coupled-tank system," *Int. J. Robot. Control Syst.*, vol. 5, no. 3, pp. 1758–1769, 2025.

[3] M. H. Jali, A. Ibrahim, R. Ghazali *et al.,* "Robust control approach of SISO coupled tank system," *Int. J. Adv. Comput. Sci. Appl.*, vol. 12, no. 1, pp. 188–193, 2021.

[4] R. Al-Majeez, K. Al-Badri, H. Al-Khazraji *et al.,* "Design of a backstepping control and synergetic control for an interconnected twin-tanks system: A comparative study," *Int. J. Robot. Control Syst.*, vol. 4, no. 4, pp. 2041–2054, 2024.

[5] I. Aranda-Cetraro, G. Pérez-Zúñiga, R. Rivas-Pérez *et al.,* "Nonlinear robust control by a modulating-function-based backstepping super-twisting controller for a quadruple tank system," *Sensors*, vol. 23, no. 11, 5222, 2023.

[6] X. Meng, H. Yu, H. Wu *et al.,* "Disturbance observer-based integral backstepping control for a two-tank liquid level system subject to external disturbances," *Math. Probl. Eng.*, vol. 2020, 6801205, 2020.

[7] X. Meng, H. Yu, J. Zhang *et al.,* "Disturbance observer-based feedback linearization control for a quadruple-tank liquid level system," *ISA Trans.*, vol. 122, pp. 146–162, 2022.

[8] X. Meng, H. Yu, T. Xu *et al.,* "Disturbance observer and L2-gain-based state error feedback linearization control for the quadruple-tank liquid-level system," *Energies*, vol. 13, no. 20, 5500, 2020.

[9] X. Meng, H. Yu, J. Zhang *et al.,* "Liquid level control of four-tank system based on active disturbance rejection technology," *Measurement*, vol. 175, 109146, 2021.

[10] A. Osman, T. Kara, and M. Arıcı, "Robust adaptive control of a quadruple tank process with sliding mode and pole placement control strategies," *IETE J. Res.*, vol. 69, no. 5, pp. 2412–2425, 2021.

[11] A. Abushokor and S. M. Amrr, "Model-free adaptive time-delay based estimation control for input-saturated coupled tank system: Experimental validation," *IEEE Trans. Autom. Sci. Eng*., vol. 22, pp. 19340–19351, 2025.

[12] R. Raj, A. Kumar, D. Sharma *et al.,* "TS fuzzy controller with s- and z-type MFs to control a coupled-tank system," *Mater. Today: Proc.,* vol. 80, pp. A8–A13, 2023.

[13] D. S. Bhandare, N. R. Kulkarni, and M. V. Bakshi, "Hardware implementation of a novel intelligent Fuzzy Fractional Order Proportional-Integral (FFOPI) controller for a coupled tank liquid level control system," *Sādhanā*, vol. 49, no. 4, 296, 2024.

[14] A. M. El-Nagar and M. I. Abdo, "Development of sliding mode control based on diagonal recurrent neural network for coupled tank system," *Neural Comput. Appl*., vol. 36, pp. 15279–15293, 2024.

[15] S. Zeghlache, M. Z. Ghellab, A. Djerioui *et al.,* "Adaptive fuzzy fast terminal sliding mode control for inverted pendulum-cart system with actuator faults," *Math. Comput. Simul.*, vol. 210, pp. 207–234, 2023.

[16] C. V. Kien, H. P. H. Anh, and N. N. Son, "Adaptive inverse multilayer fuzzy control for uncertain nonlinear system optimizing with differential evolution algorithm," *Appl. Intell.*, vol. 51, pp. 527–548, 2021.

[17] M. Yang, X. Zhang, Y. Xia *et al.,* "Adaptive neural network-based sliding mode control for a hydraulic rotary drive joint," *Comput. Electr. Eng.*, vol. 102, 108189, 2022.

[18] B. Li, J. Zhu, R. Zhou *et al.,* "Adaptive neural network sliding mode control for a class of SISO nonlinear systems," *Mathematics*, vol. 10, no. 7, 1182, 2022.

[19] S. Chaudhuri, R. Saha, A. Chatterjee *et al.,* "Adaptive neural-bias-sliding mode control of rugged electrohydraulic system motion by recurrent Hermite neural network," *Control Eng. Pract.*, vol. 103, 104588, 2020.

[20] J. Fu, F. Huang, and Z. Chen, "Optimization-based adaptive neural sliding mode control for nonlinear systems with fast and accurate response under state and input constraints," *J. Franklin Inst.*, vol. 359, no. 13, pp. 6735–6758, 2022.

[21] P. Singh, D. K. Giri, and A. K. Ghosh, "Robust backstepping sliding mode aircraft attitude and altitude control based on adaptive neural network using symmetric BLF," *Aerospace Sci. Technol.*, vol. 126, 107653, 2022.

[22] A. Baraean, M. Kassas, M. S. Alam *et al.,* "Physics-informed NN-based adaptive backstepping terminal sliding mode control of buck converter for PEM electrolyzer," *Heliyon*, vol. 10, no. 7, e29254, 2024.

[23] S. Han, H. Wang, Y. Tian *et al.,* "Time-delay estimation based computed torque control with robust adaptive RBF neural network compensator for a rehabilitation exoskeleton," *ISA Trans.*, vol. 97, pp. 171–181, 2020.

[24] H. Feng, Q. Song, S. Ma *et al*., "A new adaptive sliding mode controller based on the RBF neural network for an electro-hydraulic servo system," *ISA Trans.*, vol. 129, pp. 472–484, 2022.
[25] Z. Zhao and X. Jin, "Adaptive neural network-based sliding mode tracking control for agricultural quadrotor with variable payload," *Comput. Electr. Eng.*, vol. 103, 108336, 2022.
[26] N. V. Quan and N. N. Son, "Control of a DC–DC buck converter using adaptive neural network," *Electr. Eng.*, vol. 107, pp. 6815–6825, 2025.
[27] Z. Wu, B. Jiang, and Q. Gao, "State estimation and fuzzy sliding mode control of nonlinear Markovian jump systems via adaptive neural network," *J. Franklin Inst.*, vol. 359, no. 16, pp. 8974–8990, 2022.
[28] L. Shanmugam and Y. H. Joo, "Adaptive neural networks-based integral sliding mode control for T–S fuzzy model of delayed nonlinear systems," *Appl. Math. Comput.*, vol. 450, 127983, 2023.
[29] X. Su, X. Yang, and Y. Xu, "Fuzzy adaptive terminal sliding mode control based on recurrent neural network compensation for a maglev system," *Eng. Appl. Artif. Intell.*, vol. 124, 106588, 2023.
[30] X. Gong, W. Fu, X. Bian *et al.,* "Adaptive backstepping terminal sliding mode control of nonlinear system using fuzzy neural structure," *Mathematics*, vol. 11, no. 5, 1094, 2023.
[31] N. Jennan and E. M. Mellouli, "Optimal fixed-time sliding mode control for anti-lock braking systems based on fuzzy logic and neural network," *Results Eng.*, vol. 25, 103921, 2025.
[32] Q.-Q. Zhang and R.-J. Wai, "Distributed secondary control of islanded micro-grid based on adaptive fuzzy–neural-network-inherited total-sliding-mode control technique," *Int. J. Electr. Power Energy Syst.*, vol. 137, 107792, 2022.
[33] Y. Chu, C. Zhou, S. Hou *et al.,* "Self-organizing feature selection fuzzy neural network-based terminal sliding mode control for uncertain nonlinear systems," *ISA Trans.*, vol. 154, pp. 171–185, 2024.
[34] M. M. Zirkohi, "Adaptive interval type-2 fuzzy recurrent RBFNN control design using ellipsoidal membership functions with application to MEMS gyroscope," *ISA Trans.*, vol. 119, pp. 25–40, 2022.
[35] J. Hu, D. Zheng, Z.-G. Wu *et al.,* "Neural network-based adaptive second-order sliding mode control for uncertain manipulator systems with input saturation," *ISA Trans.*, vol. 136, pp. 126–138, 2023.
[36] Z. Liu, X. Gong, and J. Fei, "Nonsingular fast terminal sliding mode control of DC–DC buck converter using fuzzy neural network and disturbance observer," *Nonlinear Dyn.*, vol. 113, pp. 13389–13414, 2025
[37] J. Fei and Z. Feng, "Adaptive super-twisting sliding mode control for micro gyroscope based on double-loop fuzzy neural network structure," *Int. J. Mach. Learn. Cybern.*, vol. 12, pp. 611–624, 2021.
[38] J. Xie and J. Fei, "Adaptive fuzzy neural super-twisting control of micro gyroscope sensor," *Sci. Rep.*, vol. 14, 26192, 2024.
[39] G. Xiao, B. Liu, Y. Li *et al.,* "Hybrid neural network adaptive fuzzy sliding mode online compensatory control for robots with global stability," *Neurocomputing*, vol. 657, 131632, 2025.
[40] N. K. Nguyen, Q. V. B. Bui, Q. H. Nguyen *et al.,* "Adaptive fuzzy-neural network effectively disturbance compensate in sliding mode control for dual arm robot," *EUREKA: Phys. Eng.*, no. 2, pp. 79–93, 2024.
[41] Y.-T. Sun, B.-L. Zhang, and B. Yin, "Neural network-based adaptive sliding mode fuzzy control for riser system with mass-related parametric perturbation," *Ocean Eng.*, vol. 343, 123134, 2026.